

Scalable entanglement of remote material qubits produced by single photons via a no-energy-exchange process

Gang Li,^{*} Pengfei Zhang, and Tiancai Zhang[†]

*State Key Laboratory of Quantum Optics and Quantum Optics Devices,
and Institute of Opto-Electronics, Shanxi University, Taiyuan 030006*

Collaborative Innovation Center of Extreme Optics, Shanxi University, Taiyuan 030006

(Dated: August 15, 2016)

We propose a proposal to generate scalable entanglement of remote material qubits via no-energy-exchange interactions with single photons. A strongly-coupled cavity quantum electrodynamics (CQED) system is arranged as a single-photon-level quantum router, which routes incoming photons to different outputs based on the state of the involved material qubit. Two of the routers with qubits in their maximum superposition state are coupled together with a Mach-Zehnder-interferometer-like configuration. As a single photon transits through the system, we find the maximum entangled state between qubits is produced by finding a photon in the output mode. Remarkably, there is no energy exchanged between material qubits and photons. This ensures the possibility of purifying entangled states by using more photons in a physical situation, where loss and imperfections are inevitable. It also guarantees scalability in order to produce entanglement among multiple qubits without inducing incoherence caused by energy exchange. We analyzed the fidelity and probability of success for the proposed strongly-coupled CQED system. The expected maximum fidelity could reach over 0.9997 using only two photons in a technologically-feasible experiment. We also analyzed the scalability by providing examples for the generation of N-qubit entanglement and 3-qubit Greenberger-Horne-Zeilinger states based on the proposed technique. Our proposed method could be applied to create entanglement between multiple-node systems in a quantum network, or to generate special entangled state between remote material qubits, thereby testing the fundamentals of quantum mechanics.

PACS numbers: 03.65.Ud, 03.67.Bg, 42.50.Dv

Quantum entanglement is a key feature in quantum mechanics and has been recognized as an important resource for quantum information processing [1] and quantum measurement [2]. Entanglement of remote material qubits is essential for long distance quantum communication [3–5] and quantum networks [6]. There are several methods used to produce remote entanglement of qubits. One technique involves entangling a photon to the first material qubit and directly writing it into the second material qubit [7, 8]. Another option is the heralded protocol [4, 9], wherein two photons entangled to each of the two material qubits interfere in a 50/50 beam splitter. After passing the beam splitter, the photon states are then analyzed and finally detected with single photon detectors. Upon measuring different responses at the detectors, the states of various material qubits are projected into different entangled states [10–15]. The third way is also a heralded protocol [16], which is based on the quantum interference of two separated atomic qubits. The detection of a single photon from two atoms produces entanglement between them [17]. However, each of these methods involves energy exchange between the material qubit and the photon. Photons are usually the direct emissions of material qubits from some specific initial state. It is therefore difficult to scale up the size of the produced entangled state under these protocols because the re-initialization process would destroy the original state of the material qubits.

Cavity quantum electrodynamics (CQED) systems are

powerful devices used to produce entanglement of atoms coupled to the same cavity mode [9, 18–26]. In these systems, photons and atoms can also be used to non-destructively detect each other [27–30]. Based on the method used in [29] we demonstrate that a strongly-coupled CQED system can work exactly as a single photon quantum router, in which the route taken by an incoming photon can be directed to different output ports which are determined by the state of the material qubit. We propose a proposal to entangle two material qubits coupled to two separate cavities by means of sending and detecting single photons through two coupled CQED-based quantum routers with a certain configuration. Remarkably, there is no energy exchanged between material qubits and photons. This ensures the possibility of purifying the entangled state by using more photons in a physical situation where loss and other imperfections are inevitable. This also guarantees scalability for producing entanglement among additional qubits. Our proposed method could be applied to create entanglement between multiple-node systems in a quantum network [6], or to generate the Greenberger-Horne-Zeilinger (GHZ) state between remote material qubits, thereby testing the fundamentals of quantum mechanics [31].

We first take a strongly-coupled system with single atoms and an optical Fabry-Pérot (FP) cavity [32, 33] as a general representation for all types of CQED systems in order to describe the mechanism of a single-photon quantum router. The basic concept is shown in

the schematic of FIG. 1(a), where the cavity is comprised of two identical mirrors with transmission decay rates of $\kappa_1 = \kappa_2 = \kappa/2$, with κ representing the overall cavity decay rate. An atom with two ground states, $|\alpha\rangle$ and $|\beta\rangle$, and an excited state $|e\rangle$, which is associated with the decay rate γ , resides in the cavity mode. The atomic transition $|\beta\rangle \leftrightarrow |e\rangle$ strongly couples the cavity to the coupling efficiency g . For an incident light field with frequency $|\beta\rangle \leftrightarrow |e\rangle$ and cavity mode, the reflection amplitude and transmission can be expressed as $r = 1 - \kappa\gamma/(\kappa\gamma + g^2)$ and $t = \kappa\gamma/(\kappa\gamma + g^2)$ (refer to the Supplementary Material). If the atom is in state $|\alpha\rangle$, there is no coupling between the atom and the cavity. Thus with $g = 0$, we get $r = 0$ and $t = 1$ as the behavior of an empty cavity, as shown in FIG. 1(c) and (d). The light field will transmit through the cavity without any interactions with the atom. If the atom is in state $|\beta\rangle$, where the coupling g is then switched on, the normal mode splitting $2g$, due to atom-cavity coupling, will be much larger than the line width of the coupled system ($\gamma + \kappa$) in the strong coupling regime. The incident light field resonating with the empty cavity then becomes significantly detuned and is totally reflected. We get $r \approx 1$ and $t \approx 0$ on the strong coupling condition $g \gg \kappa, \gamma$. In both of these two cases, there is no energy exchange between atoms and photons and, in principle, the evolution of the atomic state will not be disturbed. This has been used to measure atomic states [29].

We can also see that by setting the atomic state in either $|\alpha\rangle$ or $|\beta\rangle$, the CQED system can route the incident photon in the input mode $|a_{in1}\rangle$ ($|a_{in2}\rangle$) to output modes $|a_{out2}\rangle$ ($|a_{out1}\rangle$) or $|a_{out1}\rangle$ ($|a_{out2}\rangle$), respectively. If the atom is in a coherent superposition state, $\cos\theta|\alpha\rangle + \sin\theta\exp(i\varphi)|\beta\rangle$, the system will route the input photons to both of the output ports with probabilities $\cos^2\theta$ and $\sin^2\theta$. As such, the system works exactly as a single-photon quantum router. This system is equivalent to a four-port quantum beam splitter shown in FIG. 1(b). Here we have used $|R\rangle$ and $|T\rangle$ as meaningful representations of the internal states of material qubits involved in the router. If the quantum state of a router is $|R\rangle$, photons from both input modes are reflected. In other words, the input photons in $|a_{in1}\rangle$ and $|a_{in2}\rangle$ are routed to $|a_{out1}\rangle$ and $|a_{out2}\rangle$, respectively. Otherwise, the $|T\rangle$ -state router will route photons in $|a_{in1}\rangle$ to $|a_{out2}\rangle$ and photons in $|a_{in2}\rangle$ to $|a_{out1}\rangle$ via transmission.

Quantum entanglement of two material qubits can be realized using two routers with the configuration shown in FIG. 2. Here the routers are coupled together in a Mach-Zehnder-interferometer-like configuration and two single photon detectors, D1 and D2, detect photons in two output modes. Router quantum states are initially prepared at maximum coherent superposition, i.e., $(|R_1\rangle + \exp(i\varphi_1)|T_1\rangle)/\sqrt{2}$ and $(|R_2\rangle + \exp(i\varphi_2)|T_2\rangle)/\sqrt{2}$. The overall quantum state can be expressed as a direct

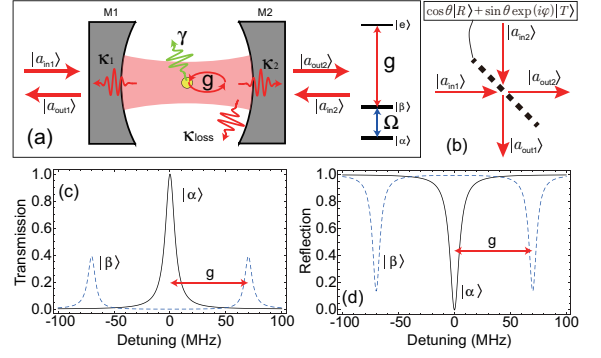


FIG. 1. (color online) (a) A schematic of a strongly-coupled CQED system with a single atom residing in the FP cavity. There are two input modes ($|a_{in1}\rangle$ and $|a_{in2}\rangle$) and two output modes ($|a_{out1}\rangle$ and $|a_{out2}\rangle$) in the system. The cavity has decay channels from transmission of the cavity mirrors (decay rates κ_1 and κ_2) and by scattering and absorption of photons in the imperfect mirror coating (decay rate κ_{loss}). The atom has two ground states, $|\alpha\rangle$ and $|\beta\rangle$, and an excited state $|e\rangle$ which is associated with the decay rate γ . The two ground states can be coupled by a microwave drive or a two-photon Raman process at the Rabi frequency Ω . The cavity is strongly coupled to the atomic transition $|\beta\rangle \leftrightarrow |e\rangle$. (b) A system equivalent to (a) with a four-port quantum router with internal states represented by $|R\rangle$ and $|T\rangle$. The transmission (c) and reflection (d) spectra for a cavity with atoms in states $|\alpha\rangle$ and $|\beta\rangle$ when the cavity is resonant to the atomic transition $|\beta\rangle \leftrightarrow |e\rangle$. It can be seen that a resonant light field will be reflected for an atom in $|\beta\rangle$ or transmitted through the cavity for an atom in $|\alpha\rangle$. Results shown in (c) and (d) were calculated using parameters with $g = 2\pi \times 70\text{MHz}$, $\gamma = 2\pi \times 3\text{MHz}$, $\kappa_1 = \kappa_2 = 2\pi \times 2.5\text{MHz}$, and $\kappa_{loss} = 0\text{MHz}$.

product of these two wave functions. By sending a single photon $|1\rangle$ into the input mode $|a_{in1}^{(1)}\rangle$, a quantum state resulting after photon transit can be expressed for the whole system as:

$$\begin{aligned} |\Psi_F\rangle &= \frac{1}{2} (|R_1, R_2\rangle + \exp(i(\varphi_1 + \varphi_2))|T_1, T_2\rangle) |a_{out1}^{(2)}, 1\rangle \\ &\quad + \frac{1}{2} (\exp(i\varphi_2)|R_1, T_2\rangle + \exp(i\varphi_1)|T_1, R_2\rangle) |a_{out2}^{(2)}, 1\rangle \\ &= |\Phi\rangle |a_{out1}^{(2)}, 1\rangle / \sqrt{2} + |\Psi\rangle |a_{out2}^{(2)}, 1\rangle / \sqrt{2}, \end{aligned} \quad (1)$$

with

$$|\Phi_2\rangle = (|R_1, R_2\rangle + \exp(i(\varphi_1 + \varphi_2))|T_1, T_2\rangle) / \sqrt{2} \quad (2)$$

and

$$|\Psi_2\rangle = (\exp(i\varphi_2)|R_1, T_2\rangle + \exp(i\varphi_1)|T_1, R_2\rangle) / \sqrt{2}. \quad (3)$$

exactly representing the two maximum entangled states for the routers. From Eq. (1) we can see that upon the event of photon detection in output mode, $|a_{out1}^{(2)}\rangle$ or $|a_{out2}^{(2)}\rangle$, the router state collapses into $|\Phi_2\rangle$ or $|\Psi_2\rangle$, respectively. This can be understood as a detected photon

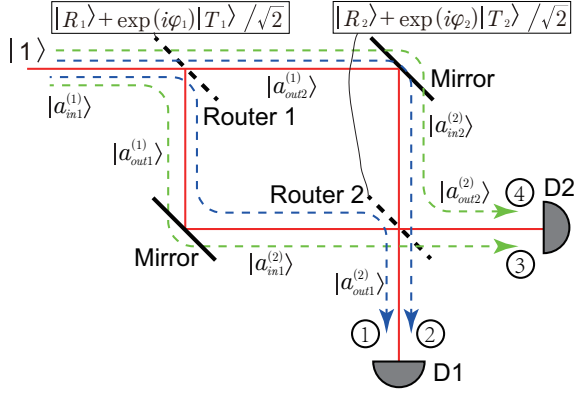


FIG. 2. (color online) The proposed method for producing entangled states with two quantum routers. Two routers are coupled together with a Mach-Zehnder-interferometer-like configuration and are prepared in their maximum superposition states. A photon is sent into the system and, upon detection, results in photons at two output modes. The perfectly-entangled states shown in Eqs. (2) and (3) can then be recovered.

in $|a_{out1}^{(2)}\rangle$ ($|a_{out2}^{(2)}\rangle$) cannot be distinguished from path 1 or path 2 (3 or 4), as shown in FIG. 2. As such, a photon detection event within D1 (D2) will lead to entangled state generation. The probability of detecting a single photon at either of these two output ports is 0.5, which implies the probability of preparing each maximum entangled state is 50%. It should be emphasized that in most CQED experiments local operations can be applied on material qubits, such as ground state manipulation of a single atom either by a 2-photon Raman process [34] or microwave driving [35]. Thus, by applying a local π -rotation and a phase shift on either of the routers, both $|\Phi_2\rangle$ and $|\Psi_2\rangle$ can be converted into each other. So, in theory, purely entangled states $|\Phi_2\rangle$ can be prepared with a probability of 100% upon clicking D1 or additional local operations on any of the routers associated with a click of D2, and similarly for $|\Psi_2\rangle$ preparation.

We now consider a real situation to demonstrate the feasibility of the proposed proposal where unexpected losses and asymmetric cavity behavior are taken into account. Losses are due to scattering and absorption of photons by imperfect mirror coatings and asymmetric behavior of the cavity is due to an imbalance of the two cavity mirrors. The achievable coupling strength g is also a finite number which is not arbitrary bigger than γ and κ . All these factors lead to a deterioration in cavity reflectivity and transmissivity. The cavity decay rate from M1 (M2) was set to $\kappa_{1(2)}$ and the total extra decay rate was κ_{loss} . The cavity reflectivity and transmissivity for an atom in state $|\beta\rangle$ then need to be modified as $r_i = 1 - 2\kappa_i\gamma/(\kappa\gamma + g^2)$ and $t_1 = t_2 = 2\sqrt{\kappa_1\kappa_2\gamma}/(\kappa\gamma + g^2)$, with $i = 1(2)$ representing the reflectivity of the input mode $|a_{in,1}\rangle$ ($|a_{in,2}\rangle$). In order to distinguish the reflectivity (transmissivity) for different cavities, qubit states

and input modes were assumed to follow the notation $r_{s,i}^{(n)}$ ($t_{s,i}^{(n)}$), where s represents the atomic state $|\alpha\rangle$ or $|\beta\rangle$, i the input mode $|a_{in,1}\rangle$ or $|a_{in,2}\rangle$, and n the cavity number. By following our proposal, we can acquire the atomic state when a single photon is injected into the system and D1 is clicked:

$$|\Psi_{21}^1\rangle = \frac{1}{2\sqrt{P_{21}^1}} (A1|\alpha_1\alpha_2\rangle + B1\exp i(\varphi_1 + \varphi_2)|\beta_1\beta_2\rangle + C1\exp i\varphi_2|\alpha_1\beta_2\rangle + D1\exp i\varphi_1|\beta_1\alpha_2\rangle), \quad (4)$$

with coefficients $A1 = r_{\alpha,1}^{(1)}r_{\alpha,1}^{(2)} + t_{\alpha,1}^{(1)}t_{\alpha,2}^{(2)}$, $B1 = r_{\beta,1}^{(1)}r_{\beta,1}^{(2)} + t_{\beta,1}^{(1)}t_{\beta,2}^{(2)}$, $C1 = r_{\alpha,1}^{(1)}r_{\beta,1}^{(2)} + t_{\alpha,1}^{(1)}t_{\beta,2}^{(2)}$, and $D1 = r_{\beta,1}^{(1)}r_{\alpha,1}^{(2)} + t_{\beta,1}^{(1)}t_{\alpha,2}^{(2)}$. $P_{21}^1 = (A1^2 + B1^2 + C1^2 + D1^2)/4$ is the probability of detecting a photon in output mode $|a_{out,1}^{(2)}\rangle$. The fidelity of this state to the maximum entangled state $|\Phi\rangle = (|\alpha_1\alpha_2\rangle + |\beta_1\beta_2\rangle)/\sqrt{2}$ is then

$$F_{21}^1 = \sqrt{\frac{(A1 + B1)^2}{2(A1^2 + B1^2 + C1^2 + D1^2)}}, \quad (5)$$

which is always less than one except when $A1 = B1$ and $C1 = D1 = 0$ in the ideal case, $t_{\alpha,i}^{(n)} = r_{\beta,i}^{(n)} = 1$ and $r_{\alpha,i}^{(n)} = t_{\beta,i}^{(n)} = 0$ ($n = i = 1, 2$). Due to unexpected losses, κ_{loss} and limited coupling strength g , the values of $C1$ and $D1$ are never zero in a real situation. These two values increase with an increase in κ_{loss} or a decrease in g . Consequently, the fidelity given in Eq. (5) will also decrease. However, as long as $C1$ and $D1$ can be controlled by coefficients smaller than $A1$ and $B1$, the fidelity is expected to improve by simply sending more photons into the system and detecting them individually in output mode $|a_{out,2}\rangle$.

After n ($n > 1$) photons are detected in $|a_{out,1}^{(2)}\rangle$, the wave function for the two atoms collapses into

$$|\Psi_{21}^n\rangle = \frac{1}{\sqrt{P_{21}^n}} (A1^n|\alpha_1\alpha_2\rangle + B1^n\exp i(\varphi_1 + \varphi_2)|\beta_1\beta_2\rangle + C1^n\exp i\varphi_2|\alpha_1\beta_2\rangle + D1^n\exp i\varphi_1|\beta_1\alpha_2\rangle), \quad (6)$$

where

$$P_{21}^n = A1^{2n} + B1^{2n} + C1^{2n} + D1^{2n} \quad (7)$$

is the probability of detecting the n th photon after $n - 1$ photons have been detected in the same output mode $|a_{out,1}^{(2)}\rangle$. As such, the probability of detecting all n photons is $P_1 = \prod_n P_{21}^n$. The fidelity given in Eq. (6) then becomes:

$$F_{21}^n = \sqrt{\frac{(A1^n + B1^n)^2}{2(A1^{2n} + B1^{2n} + C1^{2n} + D1^{2n})}}. \quad (8)$$

Depending on photon clicks in another output mode $|a_{out,2}^{(2)}\rangle$, we can get similar results to generate the entan-

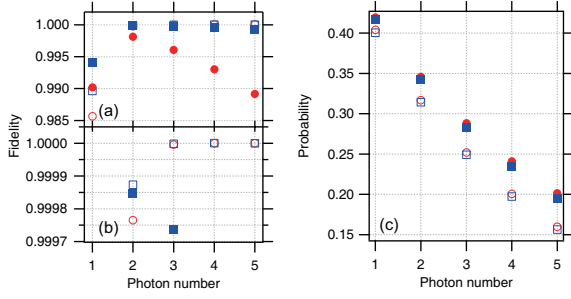


FIG. 3. (color online) (a) The fidelity of the two-atom entangled state versus the photon number used to produce the entanglement for two of the feasible CQED setups, arranged as shown in FIG. 2. (b) An enlarged region from figure (a). Blue squares represent the fidelity of $|\Psi_{21}^n\rangle$ in Eq. (8) and red circles indicate $|\Phi_{22}^n\rangle$ in Eq. (10). The distinction between solid and open points is that the former is calculated with $g^{(1)} = g^{(2)} = 2\pi \times 20$ MHz, whereas the latter is optimized for values of $g_{\text{opt}}^{(1)} = 2\pi \times 14.8$ MHz and $g_{\text{opt}}^{(2)} = 2\pi \times 16.7$ MHz as discussed in the main text. Other parameters include: $\gamma^{(1)} = \gamma^{(2)} = 2\pi \times 3$ MHz, $\kappa_1^{(1)} = 2\pi \times 2.4$ MHz, $\kappa_2^{(1)} = 2\pi \times 2.3$ MHz, $\kappa_1^{(2)} = 2\pi \times 2.6$ MHz, $\kappa_2^{(2)} = 2\pi \times 2.7$ MHz, and $\kappa_{\text{loss}}^{(1)} = \kappa_{\text{loss}}^{(2)} = 2\pi \times 0.3$ MHz [36]. (c) Probabilities of success for the two-atom entangled state versus photon numbers. The blue squares and red circles correspond to the states $|\Psi_{21}^n\rangle$ and $|\Phi_{22}^n\rangle$, respectively. The distinction between solid and open data points and parameters are the same as in (a) and (b).

gled state $|\Psi\rangle = (|\beta_1, \alpha_2\rangle + |\alpha_1, \beta_2\rangle) / \sqrt{2}$. After successively detecting n ($n > 1$) photons with D2, the state and fidelity are given by:

$$|\Phi_{22}^n\rangle = \frac{1}{\sqrt{P_{22}^n}} (A2^n |\alpha_1 \alpha_2\rangle + B2^n \exp i(\varphi_1 + \varphi_2) |\beta_1 \beta_2\rangle + C2^n \exp i\varphi_2 |\alpha_1 \beta_2\rangle + D2^n \exp i\varphi_1 |\beta_1 \alpha_2\rangle), \quad (9)$$

and

$$F_{22}^n = \sqrt{\frac{(C2^n + D2^n)^2}{2(A2^{2n} + B2^{2n} + C2^{2n} + D2^{2n})}}, \quad (10)$$

where the four coefficients $A2$, $B2$, $C2$ and $D2$ are defined as the reflectivity and transmissivity of the cavity for different settings (see details in the supplementary material).

Changes in the fidelity state [Eqs. (8) and (10)] are plotted versus the injected and detected photon numbers in FIG. 3(a) and (b) with solid circles and squares. It is remarkable that successive detection of even 2 photons in each output mode substantially improved the fidelity. Additional photons do not improve it further. This is because cavities with $\kappa_{\text{loss}} < \kappa_1, \kappa_2$ and $g > \kappa, \gamma$ can guarantee $A1, B1 > C1, D1$ and $C2, D2 > A2, B2$. Thus, by using more photons, the $C1^n$ - and $D1^n$ - terms in Eq. (6) as well as the $A2^n$ - and $B2^n$ - terms in Eq. (9) become

smaller and the fidelities are expected to continue rising. However, since $A1 \neq B1$ and $C2 \neq D2$, the difference between $A1^n$ and $B1^n$ ($C2^n$ and $D2^n$) will also be enlarged, separating the final states from the maximum entangled states. In order for the fidelities to continue increasing with photon number, the conditions $A1 = B1$ and $C2 = D2$ need to be fulfilled.

Fortunately, in a typical FP cavity-based CQED system, the coupling g can be tuned by intentionally changing the relative position of the atom with respect to the cavity mode. This provides a way to tune the cavity reflectivity r_β and transmissivity t_β and eventually reach the optimal condition $A1 = B1$ and $C2 = D2$. In our example, the optimal couplings are $g_{\text{opt}}^{(1)} = 2\pi \times 14.8$ MHz and $g_{\text{opt}}^{(2)} = 2\pi \times 16.7$ MHz. Optimized fidelity is plotted versus photon number in FIG. 3 (a) and (b) with open circles and squares. Due to a decrease in the coupling strength with the optimized condition, the fidelity upon single photon detection also decreases slightly compare to the unoptimized condition. It keeps increasing, however, as more photons are used. The fidelity is higher than 0.9997 with 2 photons. However, improved fidelity is accompanied by a trade-off in lower probabilities, which are shown in FIG. 3(c). Since the two produced entangled states can convert into each other through local operations, this system can produce any of the entangled states shown in Eqs. (2) and (3) with a fidelity over 0.9997 by sending and successively detecting 2 photons with a probability of ~ 0.64 .

Because there is no energy exchange between involved material qubits and incident photons, the proposed method could be scaled up to entangle more material qubits. FIG. 4 shows two configurations that could be used to produce different types of entangled states among 3 or more qubits within the routers. In FIG. 4(a), a cascade configuration of 3 quantum routers is displayed, where two photon detectors are used. The three involved qubits, initially prepared in their maximum superposition state $|R_i\rangle + \exp i\phi_i |T_i\rangle$ ($i = 1, 2, 3$), can be entangled by sending and detecting single photons in the output modes. When D1 or D2 is clicked, the entangled state of

$$|\Phi_3\rangle = (|R_3\rangle|\Phi_2\rangle + \exp i\varphi_3 |T_3\rangle|\Psi_2\rangle) / \sqrt{2} \quad (11)$$

or

$$|\Psi_3\rangle = (|R_3\rangle|\Psi_2\rangle + \exp i\varphi_3 |T_3\rangle|\Phi_2\rangle) / \sqrt{2} \quad (12)$$

can be prepared with $|\Phi_2\rangle$ and $|\Psi_2\rangle$ given by Eqs. (2) and (3). This can also be explained as a click of D1 (D2) cannot distinguish photon paths among 1-4 (5-8), as shown in FIG. 4(a), then produce the corresponding entanglement. This cascade configuration could be scaled up further as shown in the inset of FIG. 4(a) to produce corresponding entangled states among the N quantum routers.

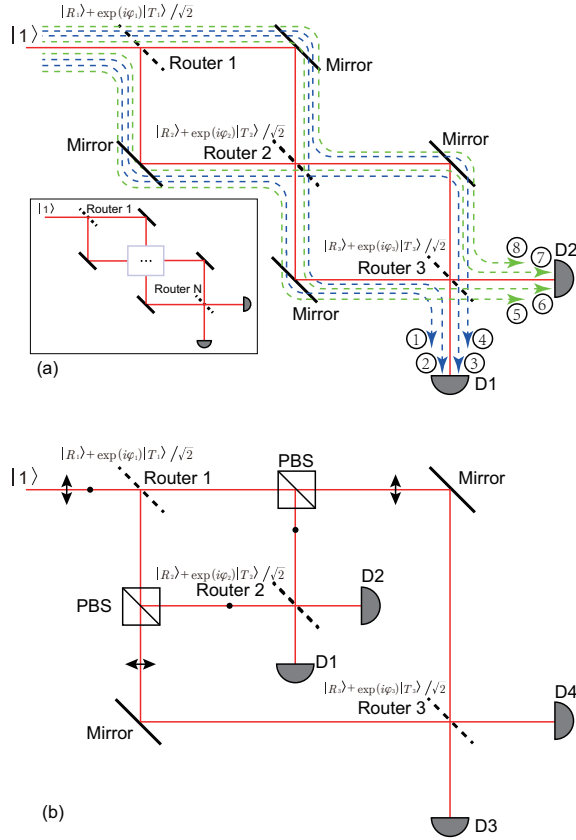


FIG. 4. (color online) (a) A schematic for generation of a 3 router-entangled state. The inset image is a schematic scaled up for an N-router entangled state. (b) A schematic for generation of a GHZ state among the 3 routers where photons with orthogonal polarizations are used.

By following a similar process, a GHZ state with three qubits could be realized if we consider the polarization of photons, as shown in FIG. 4(b). Detectors D1 and D2 (D3 and D4) respond to photons with vertical (horizontal) polarization. Two polarization beam splitters (PBS) are used to connect router 1 to router 2 (3) by photons with vertical (horizontal) polarization. After a click of D1 or D2 and a local operation on a qubit in router 2, a maximum entangled state [Eq. (2)] is produced between routers 1 and 2. Then by using single photons with horizontal polarization as the input, a click of D3 or D4 and a corresponding local operation on qubits in router 3 will produce a maximum entangled state $(|R_1, R_3\rangle + \exp i(\varphi_1 + \varphi_3)|T_1, T_3\rangle) / \sqrt{2}$ between router 1 and router 3. The overall state is simply a GHZ state $|\text{GHZ}\rangle = (|R_1, R_2, R_3\rangle + \exp i(\varphi_1 + \varphi_2 + \varphi_3)|T_1, T_2, T_3\rangle) / \sqrt{2}$ with three qubits.

In conclusion, we have proposed a proposal to entangle multiple material qubits produced by detection of single photons. Our method is based on two coupled CQED systems working in a no-energy-exchange condi-

tion where the paths of single photon flow depend on the quantum state of material qubits involved in the CQED system. The detection of single photons in the output modes will therefore mix some of the paths and result in the entanglement of material qubits. There is no energy exchange between material qubits and photons which guarantees continuity and coherence of material qubits during an interaction process. This is completely different than conventional protocols and greatly improves the viability of resulting entangled states, simplifying experimental difficulty. This advantage also ensures the possibility of purifying entangled states by using more photons and the scalability to produce entanglement between more qubits. In addition to the discussed CQED system, based on an FP cavity, the proposed method could also be implemented in other micro- or nano-optical systems. These include single atoms strongly coupled to toroid cavities [37], microspheres [38], photonic crystal waveguides [39, 40], nanofiber cavities [41], and fiber bottle micro-resonators [42], as well as superconducting qubits and quantum dots strongly coupled to various cavities [43–48].

This work was supported by the Major State Basic Research Development Program of China (Grant No. 2012CB921601) and the National Natural Science Foundation of China (Grant No. 61275210, 61227902, and 91336107).

* gangli@sxu.edu.cn

† tczhang@sxu.edu.cn

- [1] M. A. Nielsen and I. L. Chuang, *Quantum Computation and Quantum Information* (Cambridge University Press, 2000).
- [2] C. F. Roos, M. Chwalla, K. Kim, M. Riebe, and R. Blatt, *Nature* **443**, 316 (2006).
- [3] H.-J. Briegel, W. Dür, J. I. Cirac, and P. Zoller, *Phys. Rev. Lett.* **81**, 5932 (1998).
- [4] L.-M. Duan, M. D. Lukin, J. I. Cirac, and P. Zoller, *Nature* **414**, 413 (2001).
- [5] N. Sangouard, C. Simon, H. de Riedmatten, and N. Gisin, *Rev. Mod. Phys.* **83**, 33 (2011).
- [6] H. J. Kimble, *Nature* **453**, 1023 (2008).
- [7] S. Ritter, C. Nolleke, C. Hahn, A. Reiserer, A. Neuzner, M. Uphoff, M. Mücke, E. Figueroa, J. Bochmann, and G. Rempe, *Nature* **484**, 195 (2012).
- [8] D. N. Matsukevich, T. Chanelière, S. D. Jenkins, S.-Y. Lan, T. A. B. Kennedy, and A. Kuzmich, *Phys. Rev. Lett.* **96**, 030405 (2006).
- [9] L.-M. Duan and H. J. Kimble, *Phys. Rev. Lett.* **90**, 253601 (2003).
- [10] C. W. Chou, H. de Riedmatten, D. Felinto, S. V. Polyakov, S. J. van Enk, and H. J. Kimble, *Nature* **438**, 828 (2005).
- [11] J. Hofmann, M. Krug, N. Ortegel, L. Gérard, M. Weber, W. Rosenfeld, and H. Weinfurter, *Science* **337**, 72 (2012).
- [12] K. C. Lee, M. R. Sprague, B. J. Sussman, J. Nunn,

- N. K. Langford, X.-M. Jin, T. Champion, P. Michelberger, K. F. Reim, D. England, D. Jaksch, and I. A. Walmsley, *Science* **334**, 1253 (2011).
- [13] Z.-S. Yuan, Y.-A. Chen, B. Zhao, S. Chen, J. Schmiedmayer, and J.-W. Pan, *Nature* **454**, 1098 (2008).
- [14] D. L. Moehring, P. Maunz, S. Olmschenk, K. C. Younge, D. N. Matsukevich, L.-M. Duan, and C. Monroe, *Nature* **449**, 68 (2007).
- [15] C.-W. Chou, J. Laurat, H. Deng, K. S. Choi, H. de Riedmatten, D. Felinto, and H. J. Kimble, *Science* **316**, 1316 (2007).
- [16] C. Cabrillo, J. I. Cirac, P. García-Fernández, and P. Zoller, *Phys. Rev. A* **59**, 1025 (1999).
- [17] L. Slodička, G. Hétet, N. Röck, P. Schindler, M. Hennrich, and R. Blatt, *Phys. Rev. Lett.* **110**, 083603 (2013).
- [18] J. Busch, S. De, S. S. Ivanov, B. T. Torosov, T. P. Spiller, and A. Beige, *Phys. Rev. A* **84**, 022316 (2011).
- [19] B. Casabone, A. Stute, K. Friebe, B. Brandstätter, K. Schüppert, R. Blatt, and T. E. Northup, *Phys. Rev. Lett.* **111**, 100505 (2013).
- [20] M. J. Kastoryano, F. Reiter, and A. S. Sørensen, *Phys. Rev. Lett.* **106**, 090502 (2011).
- [21] E. Solano, G. S. Agarwal, and H. Walther, *Phys. Rev. Lett.* **90**, 027903 (2003).
- [22] S. Osnaghi, P. Bertet, A. Auffeves, P. Maioli, M. Brune, J. M. Raimond, and S. Haroche, *Phys. Rev. Lett.* **87**, 037902 (2001).
- [23] S.-B. Zheng and G.-C. Guo, *Phys. Rev. Lett.* **85**, 2392 (2000).
- [24] E. Hagley, X. Maitre, G. Nogues, C. Wunderlich, M. Brune, J. M. Raimond, and S. Haroche, *Phys. Rev. Lett.* **79**, 1 (1997).
- [25] T. Pellizzari, S. A. Gardiner, J. I. Cirac, and P. Zoller, *Phys. Rev. Lett.* **75**, 3788 (1995).
- [26] K. Härkönen, F. Plastina, and S. Maniscalco, *Phys. Rev. A* **80**, 033841 (2009).
- [27] G. Nogues, A. Rauschenbeutel, S. Osnaghi, M. Brune, J. M. Raimond, and S. Haroche, *Nature* **400**, 239 (1999).
- [28] C. Guerlin, J. Bernu, S. Deleglise, C. Sayrin, S. Gleyzes, S. Kuhr, M. Brune, J.-M. Raimond, and S. Haroche, *Nature* **448**, 889 (2007).
- [29] J. Volz, R. Gehr, G. Dubois, J. Esteve, and J. Reichel, *Nature* **475**, 210 (2011).
- [30] A. Reiserer, S. Ritter, and G. Rempe, *Science* **342**, 1349 (2013).
- [31] D. M. Greenberger, “GHZ (Greenberger-Horne-Zeilinger) theorem and GHZ states,” in *Compendium of Quantum Physics*, edited by D. Greenberger, K. Hentschel, and F. Weinert (Springer Berlin Heidelberg, Berlin, Heidelberg, 2009) pp. 258–263.
- [32] A. Boca, R. Miller, K. M. Birnbaum, A. D. Boozer, J. McKeever, and H. J. Kimble, *Phys. Rev. Lett.* **93**, 233603 (2004).
- [33] P. Maunz, T. Puppe, I. Schuster, N. Syassen, P. W. H. Pinkse, and G. Rempe, *Phys. Rev. Lett.* **94**, 033002 (2005).
- [34] Z.-H. Wang, G. Li, Y.-L. Tian, and T.-C. Zhang, *Frontiers of Physics* **9**, 634 (2014).
- [35] T. Xia, M. Lichtman, K. Maller, A. W. Carr, M. J. Piotrowicz, L. Isenhower, and M. Saffman, *Phys. Rev. Lett.* **114**, 100503 (2015).
- [36] Here we adapt strong coupling CQED systems with single Rubidium atoms and FP cavity. The corresponding parameters are: cavity length $l^{(1)} = l^{(2)} = 147 \mu\text{m}$, curvature radius of all cavity mirrors $R = 5 \text{ cm}$, Finesse of cavities $F^{(1)} = 102000$, $F^{(2)} = 93000$, transmission losses $l_1^{(1)} = 30 \text{ ppm}$, $l_2^{(1)} = 28.3 \text{ ppm}$, $l_1^{(2)} = 31.4 \text{ ppm}$, $l_2^{(2)} = 32.6 \text{ ppm}$, scattering and absorption losses of mirror coatings $l_{\text{loss}}^{(1)} = 3.7 \text{ ppm}$, $l_{\text{loss}}^{(2)} = 3.6 \text{ ppm}$, atomic decay rate associated with $5S_{1/2}F = 3 \rightarrow 5P_{3/2}F = 4$ $\gamma = 3\text{MHz}$.
- [37] B. Dayan, A. S. Parkins, T. Aoki, E. P. Ostby, K. J. Vahala, and H. J. Kimble, *Science* **319**, 1062 (2008).
- [38] I. Shomroni, S. Rosenblum, Y. Lovsky, O. Bechler, G. Guendelman, and B. Dayan, *Science* **345**, 903 (2014).
- [39] T. G. Tiecke, J. D. Thompson, N. P. de Leon, L. R. Liu, V. Vuletic, and M. D. Lukin, *Nature* **508**, 241 (2014).
- [40] A. Goban, C.-L. Hung, J. D. Hood, S.-P. Yu, J. A. Muniz, O. Painter, and H. J. Kimble, *Phys. Rev. Lett.* **115**, 063601 (2015).
- [41] S. Kato and T. Aoki, *Phys. Rev. Lett.* **115**, 093603 (2015).
- [42] D. O’Shea, C. Junge, J. Volz, and A. Rauschenbeutel, *Phys. Rev. Lett.* **111**, 193601 (2013).
- [43] I.-C. Hoi, C. M. Wilson, G. Johansson, T. Palomaki, B. Peropadre, and P. Delsing, *Phys. Rev. Lett.* **107**, 073601 (2011).
- [44] J. Johansson, S. Saito, T. Meno, H. Nakano, M. Ueda, K. Semba, and H. Takayanagi, *Phys. Rev. Lett.* **96**, 127006 (2006).
- [45] A. Wallraff, D. I. Schuster, A. Blais, L. Frunzio, R.-S. Huang, J. Majer, S. Kumar, S. M. Girvin, and R. J. Schoelkopf, *Nature* **431**, 162 (2004).
- [46] D. Englund, A. Faraon, I. Fushman, N. Stoltz, P. Petroff, and J. Vuckovic, *Nature* **450**, 857 (2007).
- [47] K. Hennessy, A. Badolato, M. Winger, D. Gerace, M. Atature, S. Gulde, S. Falt, E. L. Hu, and A. Imamoglu, *Nature* **445**, 896 (2007).
- [48] J. M. Fink, M. Goppl, M. Baur, R. Bianchetti, P. J. Leek, A. Blais, and A. Wallraff, *Nature* **454**, 315 (2008).

Supplemental Materials: Scalable entanglement of remote material qubits produced by single photons via a no-energy-exchange process

REFLECTIVITIES AND TRANSMISSIVITIES OF A FP CAVITY IN CAVITY QED SYSTEM

The reflectivity and transmissivity of an FP cavity can be obtained by solving the master equation driven by a coherent light source. For a cavity system with a single atom strongly coupled with the mode [see FIG. 1 (a)], the Hamiltonian is given by:

$$H = \hbar g(|\beta\rangle\langle e|a^\dagger + |e\rangle\langle\beta|a) \quad (S1)$$

where g is the coupling efficiency, a and a^\dagger are the annihilation and creation operators for the intra-cavity field, and $|\beta\rangle$ and $|e\rangle$ are two atomic states coupled to the cavity mode. If a weak coherent light source $a_{\text{in},1}$ is incident from the mirror M1, the dynamics of the intra-cavity field a are then described by the Heisenberg-Langevin equation,

$$\dot{a} = -\frac{i}{\hbar}[a, H] - \kappa a + \sqrt{2\kappa_1}a_{\text{in},1}, \quad (S2)$$

where a is the amplitude of the intra-cavity field, κ_1 is the transmission decay rate from mirror M1, $\kappa = \kappa_1 + \kappa_2 + \kappa_{\text{loss}}$ is the total decay rate for the cavity with κ_{loss} representing the overall scattering and absorption loss rates, and κ_2 is the transmission decay rate for mirror M2. Simultaneously, we also have relationships between the input and output field for the cavity with

$$a_{\text{out},1} + a_{\text{in},1} = \sqrt{2\kappa_1}a \quad (S3)$$

and

$$a_{\text{out},2} + a_{\text{in},1} = \sqrt{2\kappa_2}a, \quad (S4)$$

where $a_{\text{out},1}$ and $a_{\text{out},2}$ are the output fields for the cavity from M1 and M2, respectively. Under the weak excitation approximation, where the excitation of an atom is negligibly small, Eqs. (S2-S4) can be solved analytically. The coefficients for reflection and transmission of the input $a_{\text{in},1}$ can then be obtained with

$$r_1 = \frac{a_{\text{out},1}}{a_{\text{in},1}} = 1 - \frac{2\kappa_1(i\Delta_a + \gamma)}{(i\Delta_c + \kappa)(i\Delta_a + \gamma) + g^2} \quad (S5)$$

and

$$t_1 = \frac{a_{\text{out},2}}{a_{\text{in},1}} = \frac{2\sqrt{\kappa_1\kappa_2}(i\Delta_a + \gamma)}{(i\Delta_c + \kappa)(i\Delta_a + \gamma) + g^2}, \quad (S6)$$

here Δ_a and Δ_c are the frequency detunings for the incident field with respect to resonance of atomic transitions in the cavity. In our case $\Delta_a = \Delta_c = 0$, so the reflectivity and transmissivity can be simplified as

$$r_1 = 1 - 2\kappa_1\gamma/(\kappa\gamma + g^2) \quad (S7)$$

and

$$t_1 = 2\sqrt{\kappa_1\kappa_2}\gamma/(\kappa\gamma + g^2) \quad (S8)$$

Using a similar method, we can recover the reflectivity of the input field $a_{\text{in},2}$ on the side of mirror M2:

$$r_2 = \frac{a_{\text{out},2}}{a_{\text{in},2}} = 1 - \frac{2\kappa_2(i\Delta_a + \gamma)}{(i\Delta_c + \kappa)(i\Delta_a + \gamma) + g^2}. \quad (S9)$$

The transmissivity takes a form similar to Eq. (S6). Since $\Delta_a = \Delta_c = 0$, the reflectivity is given by

$$r_2 = 1 - 2\kappa_2\gamma/(\kappa\gamma + g^2) \quad (S10)$$

and the transmissivity takes the same form as Eq. (S8). In the ideal case, where $\kappa_{\text{loss}} = 0$ and $\kappa_1 = \kappa_2$, the reflectivity and transmissivity are given by

$$r = 1 - \kappa\gamma/(\kappa\gamma + g^2) \quad (S11)$$

and

$$t = \kappa\gamma/(\kappa\gamma + g^2), \quad (S12)$$

they are same for inputs on both sides.

THE ENTANGLED WAVEFUNCTION AND FIDELITY IN AN EXPERIMENTAL CONFIGURATION UPON PHOTON DETECTION FOR OUTPUT PORT $|a_{\text{out}2}^{(2)}\rangle$

The two atoms in routers 1 and 2 were first prepared in their maximum superposition states. Taking into account any losses in a physical experiment, we analyzed the wavefunction and fidelity upon detection of photons by D1 in the main text. Here we give wavefunction and fidelity results upon photon detection by D2 for output port $|a_{\text{out}2}^{(2)}\rangle$.

With a single photon as the input, upon a click of D2, the atomic state will collapse to

$$|\Phi_{22}^1\rangle = \frac{1}{2\sqrt{P_{22}^1}}(A2|\alpha_1\alpha_2\rangle + B2\exp i(\varphi_1 + \varphi_2)|\beta_1\beta_2\rangle + C2\exp i\varphi_2|\alpha_1\beta_2\rangle + D2\exp i\varphi_1|\beta_1\alpha_2\rangle) \quad (\text{S13})$$

with coefficients $A2 = r_{\alpha,1}^{(1)}t_{\alpha,1}^{(2)} + t_{\alpha,1}^{(1)}r_{\alpha,2}^{(2)}$, $B2 = r_{\beta,1}^{(1)}t_{\beta,1}^{(2)} + t_{\beta,1}^{(1)}r_{\beta,2}^{(2)}$, $C2 = r_{\alpha,1}^{(1)}t_{\beta,1}^{(2)} + t_{\alpha,1}^{(1)}r_{\beta,2}^{(2)}$, $D2 = r_{\beta,1}^{(1)}r_{\alpha,1}^{(2)} + t_{\beta,1}^{(1)}r_{\alpha,2}^{(2)}$. $P_{22}^1 = (A2^2 + B2^2 + C2^2 + D2^2)/4$ is the probability of detecting the photon with D2. The fidelity of this wave function in the maximum entangled state $|\Psi\rangle = (\exp i\varphi_2|\beta_1, \alpha_2\rangle + \exp i\varphi_1|\alpha_1, \beta_2\rangle) / \sqrt{2}$ can be expressed as

$$F_{22}^1 = \sqrt{\frac{(C2 + D2)^2}{2(A2^2 + B2^2 + C2^2 + D2^2)}}. \quad (\text{S14})$$

The fidelity will be smaller than 1 due to nonzero values for $A2$ and $D2$, caused by losses in κ_{loss} and γ . The fidelity of the final wavefunction can be improved by successively injecting more photons into the system. By sequentially detecting n ($n > 1$) photons with D2, the atomic states collapse to

$$|\Phi_{22}^n\rangle = \frac{1}{\sqrt{P_{22}^n}}(A2^n|\alpha_1\alpha_2\rangle + B2^n\exp i(\varphi_1 + \varphi_2)|\beta_1\beta_2\rangle + C2^n\exp i\varphi_2|\alpha_1\beta_2\rangle + D2^n\exp i\varphi_1|\beta_1\alpha_2\rangle), \quad (\text{S15})$$

where

$$P_{22}^n = A2^{2n} + B2^{2n} + C2^{2n} + D2^{2n} \quad (\text{S16})$$

is the probability of detecting the n th photon after $n - 1$ photons have been detected for the same output $|a_{\text{out}2}^{(2)}\rangle$. The probability of recording all n photons for the output is then $P_2 = \prod_n P_{22}^n$. The fidelity of Eq. (S15) is then given by

$$F_{22}^n = \sqrt{\frac{(C2^n + D2^n)^2}{2(A2^{2n} + B2^{2n} + C2^{2n} + D2^{2n})}}. \quad (\text{S17})$$

From this equation we also observe that the fidelity can be improved further, as long as $C2 = D2$ and $C2, D2 > A2, B2$ as analyzed and described in the main text.

FIDELITY AND RESULTING PROBABILITY ANALYZE FOR A WORSE SITUATION

We also analyzed the fidelity and success probability for a less-ideal situation, where unexpected losses are larger, using single photons as the input. The results are shown in FIG. 1S. Here the related parameters were cavity length: $l^{(1)} = l^{(2)} = 147 \mu\text{m}$, radius of curvature for all cavity mirrors: $R = 5 \text{ cm}$, cavity finesse: $F^{(1)} = 102000$ and $F^{(2)} = 93000$, transmission loss: $l_1^{(1)} = 24.6 \text{ ppm}$, $l_2^{(1)} = 28.3 \text{ ppm}$, $l_1^{(2)} = 25.3 \text{ ppm}$, and $l_2^{(2)} = 29 \text{ ppm}$, scattering and absorption loss for mirror coatings: $l_{\text{loss}}^{(1)} = 8.6 \text{ ppm}$ and $l_{\text{loss}}^{(2)} = 13.3 \text{ ppm}$, and atomic decay rates associated with $5S_{1/2}F = 3 \rightarrow 5P_{3/2}F = 4$ $\gamma = 3 \text{ MHz}$.

From this figure we also observe that the overall fidelity is lower than a situation with lower losses, as in FIG. 3. The fidelity can be continually improved by optimizing the coupling efficiency between the atom and cavity to yield $A1 = B1$ and $C2 = D2$. In optimal conditions, the fidelity is larger than 0.99 using 3 photons as the input. However, due to a low coupling efficiency between the atom and cavity, the probability of success drops to 0.06-0.08. The fidelity can be improved further by using more photons but the corresponding probability of success will be lower.

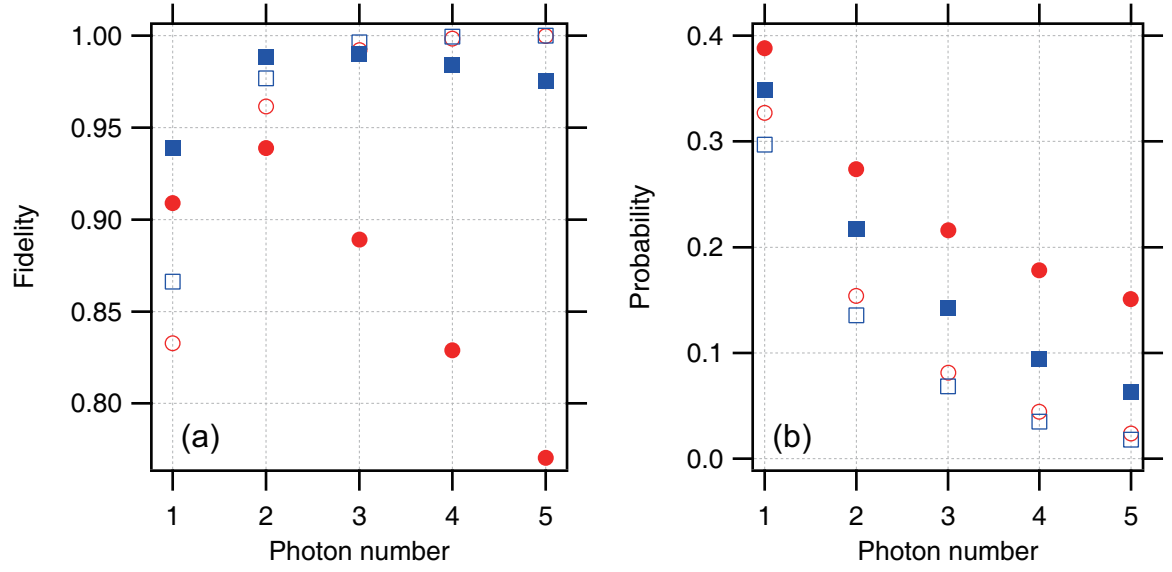


FIG. S1. (color online) (a) The fidelity of the two-atom entangled state versus the number of photons successively detected from one output port when two of the real CQED setups are arranged as shown in the schematic of FIG. 2. The blue squares were calculated with Eq. (8) and the red circles were calculated with Eq. (10). The distinction between solid and open data points is that solid points were calculated with $g^{(1)} = g^{(2)} = 2\pi \times 20$ MHz, whereas open points were calculated by setting $g_{\text{opt}}^{(1)} = 2\pi \times 8.8$ MHz and $g_{\text{opt}}^{(2)} = 2\pi \times 7.2$ MHz, where $A1 = B1$ and $C2 = D2$ are satisfied. Other parameters used in the calculations include $\gamma^{(1)} = \gamma^{(2)} = 2\pi \times 3$ MHz, $\kappa_1^{(1)} = 2\pi \times 2.0$ MHz, $\kappa_2^{(1)} = 2\pi \times 2.3$ MHz, $\kappa_{\text{loss}}^{(1)} = 0.7$ MHz, $\kappa_1^{(2)} = 2\pi \times 2.1$ MHz, $\kappa_2^{(2)} = 2\pi \times 2.4$ MHz, and $\kappa_{\text{loss}}^{(2)} = 2\pi \times 1.1$ MHz. (b) The probability of success for a two-atom entangled state versus the number of photons. In this figure, the blue squares correspond to the state shown in Eq. (6) and the red circles correspond to the state shown in Eq. (9). The distinction between solid and open data points and the parameters used for calculations are the same as in (a).